Molecular Vision 2017; 23:140-148 <http://www.molvis.org/molvis/v23/140>
Received 13 September 2016 | Accepted 16 March 2017 | Published 18 March 2017

A mutagenesis-derived *Lrp5* mouse mutant with abnormal retinal vasculature and low bone mineral density

Jeremy R. Charette,[1] Sarah E. Earp,[2,3] Brent A. Bell,[3] Cheryl L. Ackert-Bicknell,[1,4] Dana A. Godfrey,[4] Sujata Rao,[2,3] Bela Anand-Apte,[2,3] Patsy M. Nishina,[1] Neal S. Peachey[2,3,5]

[1]The Jackson Laboratory, Bar Harbor, ME; [2]Cleveland Clinic Lerner College of Medicine of Case Western Reserve University, Cleveland, OH; [3]Cole Eye Institute, Cleveland Clinic, Cleveland, OH; [4]Center for Musculoskeletal Research, Department of Orthopaedics, University of Rochester, Rochester, NY; [5]Louis Stokes Cleveland VA Medical Center, Cleveland, OH

Purpose: Familial exudative vitreoretinopathy (FEVR) is caused by mutations in the genes encoding low-density lipoprotein receptor-related protein (LRP5) or its interacting partners, namely frizzled class receptor 4 (FZD4) and norrin cystine knot growth factor (NDP). Mouse models for *Lrp5*, *Fzd4*, and *Ndp* have proven to be important for understanding the retinal pathophysiology underlying FEVR and systemic abnormalities related to defective Wnt signaling. Here, we report a new mouse mutant, *tvrm111B*, which was identified by electroretinogram (ERG) screening of mice generated in the Jackson Laboratory Translational Vision Research Models (TVRM) mutagenesis program.
Methods: ERGs were used to examine outer retinal physiology. The retinal vasculature was examined by *in vivo* retinal imaging, as well as by histology and immunohistochemistry. The *tvrm111B* locus was identified by genetic mapping of mice generated in a cross to DBA/2J, and subsequent sequencing analysis. Gene expression was examined by real-time PCR of retinal RNA. Bone mineral density (BMD) was examined by peripheral dual-energy X-ray absorptiometry.
Results: The *tvrm111B* allele is inherited as an autosomal recessive trait. Genetic mapping of the decreased ERG b-wave phenotype of *tvrm111B* mice localized the mutation to a region on chromosome 19 that included *Lrp5*. Sequencing of *Lrp5* identified the insertion of a cytosine (c.4724_4725insC), which is predicted to cause a frameshift that disrupts the last three of five conserved PPPSPxS motifs in the cytoplasmic domain of LRP5, culminating in a premature termination. In addition to a reduced ERG b-wave, *Lrp5*^{tvrm111B} homozygotes have low BMD and abnormal features of the retinal vasculature that have been reported previously in *Lrp5* mutant mice, including persistent hyaloid vessels, leakage on fluorescein angiography, and an absence of the deep retinal capillary bed.
Conclusions: The phenotype of the *Lrp5*^{tvrm111B} mutant includes abnormalities of the retinal vasculature and of BMD. This model may be a useful resource to further our understanding of the biological role of LRP5 and to evaluate experimental therapies for FEVR or other conditions associated with LRP5 dysfunction.

Mutagenesis and analysis of mice by system-specific screens has been used to understand the genes that contribute to a wide range of biological processes and diseases [1]; the use of this approach by multiple laboratories has yielded a rich array of mouse models for biomedical research [2,3]. Structural and functional screens have been used to identify mutants that impact the eye [2,4-8]. Among these, the Translational Vision Research Models (TVRM) program at the Jackson Laboratory develops new mouse models of eye disease by exposing wild-type (WT) C57BL/6J male mice to the mutagen *N*-ethyl-*N*-nitrosourea (ENU) and screening the eyes of offspring generated through a three-generation mating strategy by indirect ophthalmoscopy and/or electroretinography [6].

In this report, we describe the generation and initial characterization of a new autosomal recessive model (*tvrm111B*) caused by a mutation in the low-density lipoprotein receptor-related protein 5 (*Lrp5*) gene. Affected *tvrm111B* mice were identified via an electroretinogram (ERG) screen. The abnormal ERG phenotype was used to map the *tvrm111B* trait to chromosome 19, and further genetic analysis revealed that the phenotype is caused by a single-nucleotide insertion that affects the three terminal PPPSPxS motifs of the protein.

Our studies focused on two aspects of the *Lrp5*^{tvrm111B} phenotype, namely retinal vasculature and bone density. These factors were chosen based on the recognized role of LRP5 in canonical Wnt signaling and the phenotypes associated with mutations in *LRP5/Lrp5* in humans and mice. In humans, inactivating mutations in LRP5 cause osteoporosis pseudoglioma (OPPG) [9,10]. OPPG is an autosomal recessive disorder in which affected patients develop severe juvenile-onset osteoporosis and congenital blindness [9,10]. Other reports have linked *LRP5* mutations to familial exudative vitreoretinopathy (FEVR), a retinal condition characterized by abnormal development of the deep retinal capillary beds [11,12], or to high bone mineral density (BMD) [13,14].

Correspondence to: Neal Peachey, Cole Eye Institute, Cleveland Clinic, 9500 Euclid Avenue, Cleveland, OH 44195; Phone: (216) 445-1942; FAX: (216) 636-5046; email: peachen@ccf.org

Abnormal retinal vascular development has been described in two mutant mouse lines that carry inactivating mutations in *Lrp5* due to ENU mutagenesis or gene targeting [5,15]. In addition, Kato et al. [16] noted that *Lrp5*$^{-/-}$ mice have low bone mass and incomplete regression of the embryonic hyaloid vasculature. As described here, each of these abnormalities is recapitulated in *Lrp5*^{tvrm111B}, which will be available through The Jackson Laboratory either as mating pairs, if available, or reconstituted from cryopreserved sperm and will provide value for the study of these systems and others that involve LRP5 signaling.

METHODS

Mice and mapping: All procedures used in animal experiments were approved by the Institutional Animal Care & Use Committees of the institutions involved. Homozygous *tvrm111B* mice were identified by the TVRM mutagenesis program [6], in which male C57BL/6J mice were administered ENU in weekly injections of 80 mg/kg for 3 weeks [17]. In this program [18], ENU-treated males were mated to WT females to create generation (G) 1 offspring. Male G1 offspring were mated to WT females to generate G2 offspring, which were then mated back to their G1 fathers to generate G3 offspring; the G3 offspring were then examined by ERG [19] to identify mice with abnormal outer retinal function.

To map the *tvrm111B* locus, affected C57BL/6J mice were crossed to WT DBA/2J mice to generate filial (F) 1 mice that were heterozygous at the *tvrm111B* locus and carried a C57BL/6J and a DBA/2J allele at each locus. These F1 mice were then intercrossed to generate F2 mapping mice. F2 mice were examined by ERG, after which DNA was prepared from tail biopsies using proteinase K digestion and isopropyl alcohol extraction. DNA samples from 10 affected and 10 unaffected F2 offspring were pooled and subjected to a genome-wide scan in which 48 simple sequence length polymorphic markers that distinguish C57BL/6J and DBA/2J strains were used [20]. Once *tvrm111B* was localized to chromosome 19 and the linkage was confirmed, a total of 195 samples from *tvrm111B* F2 progeny were genotyped for markers D19Mit68 and D19Mit109 and single-nucleotide polymorphisms rs30822407 and rs30990604 to refine the map position.

Whole-exome sequencing: Genomic DNA (1 µg) was fragmented using a E220 Focused-ultrasonicator (Covaris, Woburn, MA) E220 to a range of sizes centered on 300 bp. The precapture paired-end library was constructed using the NEBNext DNA Library Prep Master Mix set for Illumina (New England BioLabs, Ipswich, MA) including a bead-based size selection to select for inserts with an average size of 300 bp followed by 18 cycles of PCR. The precapture library was hybridized to the Roche (Madison, WI) NimbleGen SeqCap EZ Mouse Exome Design (Ref #9999042611) capture probe set according to the manufacturer's instructions. The sequencing library was quantified by quantitative PCR (qPCR), pooled with three similar libraries, and sequenced

Table 1. Primers used in qRT-PCR analysis of *Lrp5*tvrm111B retina.

Gene	Primers
Lrp5	Lrp5-rtF2 AAGGGTGCTGTGTACTGGAC Lrp5-rtR2 AGAAGAGAACCTTACGGGACG
Plvap	Plvap-rtF1 GCTGGTACTACCTGCGCTATT Plvap-rtR1 CCTGTGAGGCAGATAGTCCA
Wnt7b	Wnt7b-rtF1 GGTGTGGCAGTGTACCTGCAA Wnt7b-rtR1 GTGAAGACCTCGGTGCGCT
Gja1	Gja1-rtF1 ACAGCGGTTGAGTCAGCTTG Gja1-rtR1 GAGAGATGGGGAAGGACTTGT
slc38a5	slc38a5-rtF1 CAACCTCAGCAACGCTATCAT slc38a5-rtR1 CAGGTCCAAATGCCCTCTG
Cldn5	Cldn5-rtF1 GCAAGGTGTATGAATCTGTGCT Cldn5-rtR1 GTCAAGGTAACAAAGAGTGCCA
Wnt5a	Wnt5a-rtF1 CAACTGGCAGGACTTTCTCAA Wnt5a-rtR1 CATCTCCGATGCCGGAACT
Wnt10b	Wnt10b-rtF1 GAAGGGTAGTGGTGAGCAAGA Wnt10b-rtF1 GAAGGGTAGTGGTGAGCAAGA CC
Mfsd2	Mfsd2-rtF1 AGAAGCAGCAACTGTCCATTT Mfsd2-rtR1 CTCGGCCCACAAAAAGGATAAT

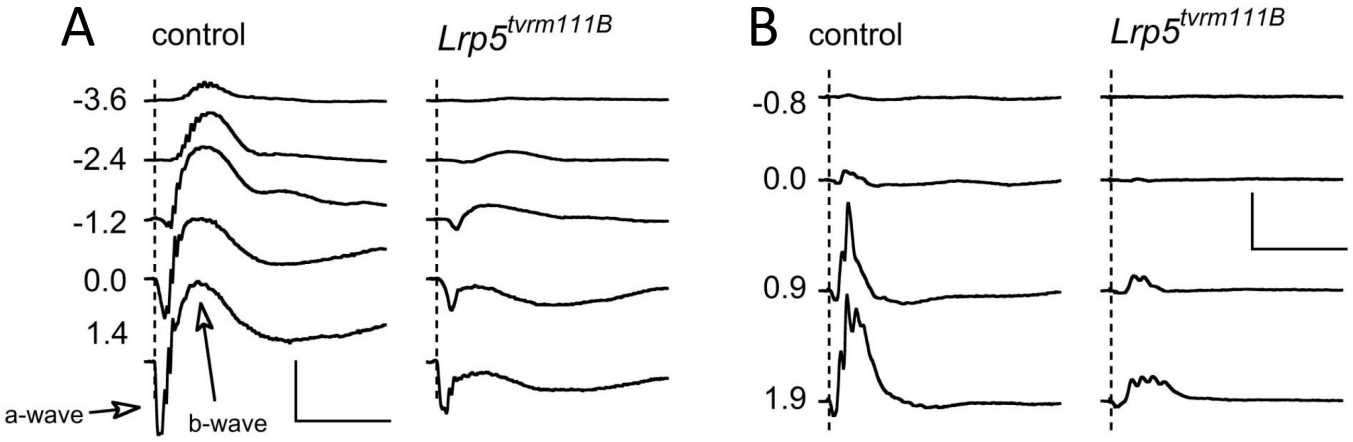

Figure 1. Electroretinogram (ERG) phenotype of *Lrp5*^{tvrm111B} mice. **A:** ERGs obtained from strobe flash stimuli presented to the dark-adapted eye from representative control (left) and *Lrp5*^{tvrm111B} (right) littermates. Scale bars indicate 500 µV and 200 ms. **B:** ERGs obtained from strobe flash stimuli superimposed against a steady adapting field from representative control (left) and *Lrp5*^{tvrm111B} (right) littermates. Values to the left of each pair of waveforms indicate flash strength (log cd sec/m^2). Scale bars indicate 200 µV and 200 ms.

on a single lane of an Illumina (San Diego, CA) HiSeq 2000 using a 2×100-base (paired-end) sequencing protocol.

Chromosome 19 enrichment and exome sequencing: The precapture library was generated as above and was hybridized to a 1M Agilent Technologies (Santa Clara, CA) SureSelect DNA Capture Array using published hybridization and posthybridization methods [21]. The array was printed with 390,033 (×2) 60-bp probes covering the NCBI build 37 coordinates from chromosome 19 (chr19) bases 3000001 to 6207730 (CM001012.1). The sequencing library was quantified by qPCR and sequenced on an Illumina MiSeq using a 2×100-base (paired-end) sequencing protocol. The resulting sequences were analyzed manually using the Integrative Genomics Viewer (Broad Institute, Cambridge, MA) to identify the cytosine insertion in *Lrp5* (c.4724_4725insC).

Sequencing: To confirm the identified mutation, we amplified and sequenced the *Lrp5* genomic DNA within the region containing the mutation in both the segregating mapping and the maintenance colonies. PCR products were purified using QIAquick PCR purification according to the manufacturer's recommendations (QIAGEN, Germantown, MD) and sequenced using BigDye Terminator Cycle Sequencing Chemistry and separated by capillary electrophoresis on Applied Biosystems 3730xl DNA Analyzer.

RNA isolation and quantitative real-time PCR: RNA was isolated from whole-eyes enucleated from P8 animals using an RNeasy Mini kit (QIAGEN). Tissues were homogenized in TRIzol (Thermofisher Scientific, Waltham, MA) and phase separated. An on-column DNase I treatment was performed and RNA was eluted using nuclease-free water. Quantitative real-time reverse transcription PCR (qRT-PCR) was performed with the iTaq Universal SYBR Green SuperMix (Bio-Rad, Hercules, CA) and gene-specific primers [22] using the CFX96 Real-Time PCR Detection System (Bio-Rad). Transcripts were analyzed by the comparative CT method using *Actb* as a normalizing gene. Error bars represent the additive propagation of error [23]. The primers used to amplify the target genes examined are listed in Table 1.

Electroretinography: After overnight dark adaptation, mice were anesthetized with ketamine (80 mg/kg) and xylazine (16 mg/kg) and their pupils were dilated with 1% tropicamide and 2.5% phenylephrine HCl eye drops. ERGs were recorded with a stainless-steel wire contacting the anesthetized (1% proparacaine HCl) corneal surface. This active electrode was referenced to a needle electrode placed in the cheek; a second needle electrode placed in the tail served as ground. Responses were differentially amplified (0.03–1,000 Hz) and stored using an LKC (Gaithersburg, MD) UTAS E-3000 signal averaging system. For examination of F2 progeny, a single stimulus condition was used (1.4 log cd s/m^2 flash presented in darkness). To characterize the *tvrm111B* phenotype, ERGs were recorded under dark-adapted stimulus conditions using flash stimuli that ranged from −3.6 to 1.2 log cd s/m^2 and under light-adapted conditions using flash stimuli that ranged from −0.8 to 1.9 log cd s/m^2 and were superimposed on a steady 20 cd/m^2 rod-desensitizing background field [24].

In vivo retinal imaging: Animal preparation, imaging, and recovery were performed as previously described [25,26]. Fluorescein angiography (FA-SLO) was performed using a Heidelberg Engineering (Franklin, MA) model HRA2 confocal scanning laser ophthalmoscope. Sodium fluorescein (Alcon Fluorescite, Fort Worth, TX) was administered

(10–20 mg/kg) via an intraperitoneal injection, and FA-SLO images of the superficial and deep capillary plexus were collected at 1, 2, 3, and 4 min postinjection [27]. Spectral domain optical coherence tomography (SDOCT) was performed using a Bioptigen (Durham, NC) model SDOIS SDOCT system. B-scans of the horizontal and vertical meridians were collected through the optic nerve at 1,000 A-scans/B-scan × 30 frames. B-scan images with dimensions of 0.4 mm (depth) × approximately 1.6 mm (width) were exported to ImageJ and coregistered and averaged using StackReg/TurboReg/Plugins [28].

Immunohistochemistry: Enucleated mouse eyes were fixed in 4% paraformaldehyde (PFA) for 30 min and washed with PBS before removal of the anterior segment and lens. PBS is purchased as a 10X powder without calcium and magnesium (Midwest Scientific, Valley Park, MO). It is diluted to 1X (pH = 7.5) with distilled water and contains KCl (2.6 mM), KH_2PO_4 (1.47 mM), NaCl (137.93 mM) and Na_2HPO_4 anhydrous (8.09 mM). Whole retinas were removed and permeabilized with 1% Triton X-100 in PBS for 45 min followed by rinsing with PBS. Retinas were incubated with Isolectin GS-IB_4 (ThermoFisher Scientific, Waltham, MA; 20 µg/ml) from *Griffonia simplicifolia*, Alexa Fluor 488 conjugate (ThermoFisher Scientific) for 48 h, washed with PBS, and mounted in Vectashield before visualization with a Leica SP8 confocal microscope (Leica Microsystems, Buffalo Grove, IL) with a 40×/1.30NA objective. Z-stack images were taken through the entire thickness of the whole mount retina and analyzed with three-dimensional (3D) modality and depth

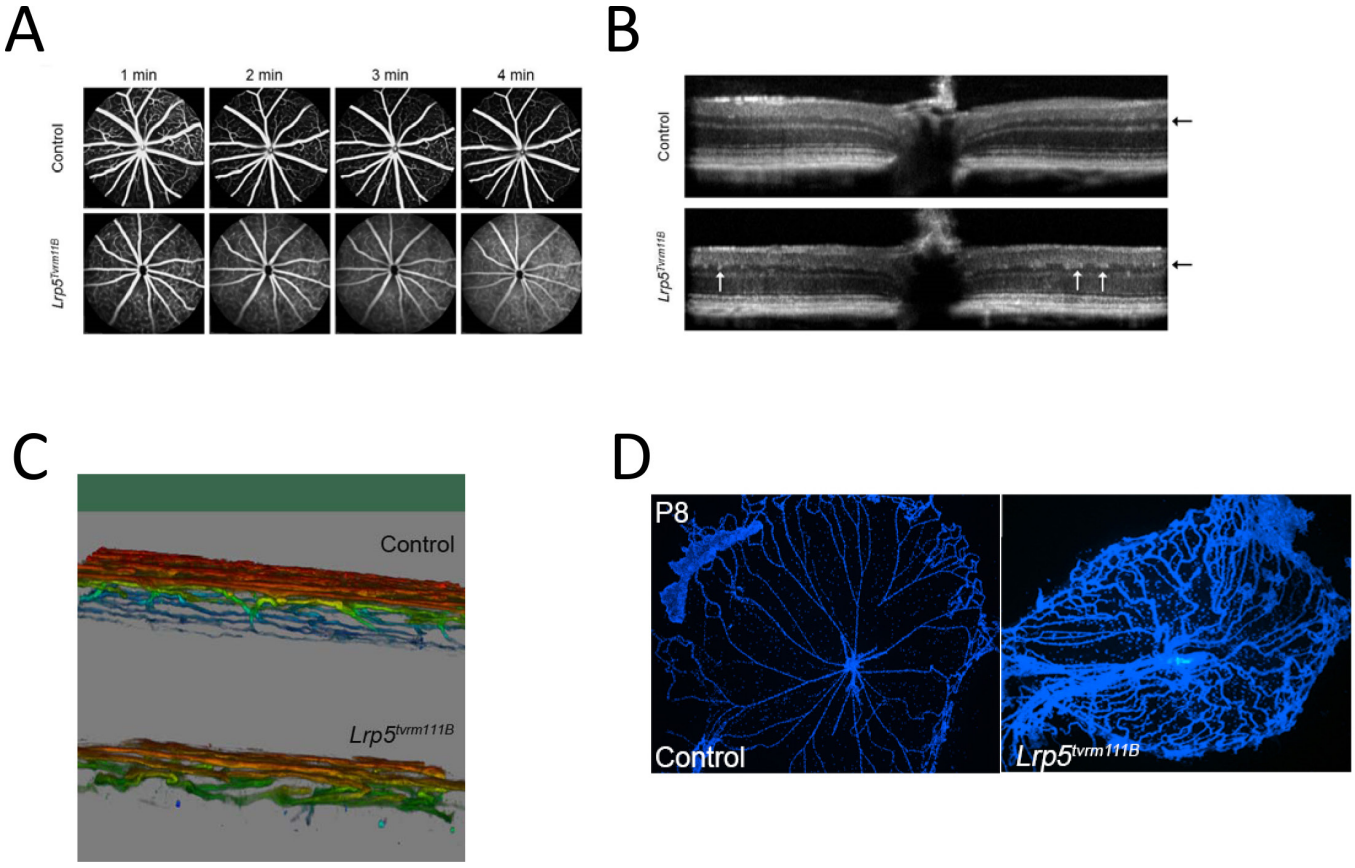

Figure 2. Retinal vascular phenotype of *Lrp5*^{tvrm111B} mice. **A:** Fluorescein angiographic images obtained 1, 2, 3, or 4 min following injection of sodium fluorescein from a control (top) and a *Lrp5*^{tvrm111B} (bottom) mouse. Fluorescein leakage is seen in the *Lrp5*^{tvrm111B} images. **B:** Optical coherence tomography (OCT) cross-sections of the control (top) and *Lrp5*^{tvrm111B} (bottom) retina. Arrows indicate altered profiles of capillary beds in the *Lrp5*^{tvrm111B} retina. All retinal lamina are present and otherwise normal with exception to (a) the transition between inner plexiform layer and inner nuclear layer (black arrows) which denotes the limit of penetration of the retinal vasculature (white arrows) within the mutant, and (b) an approximately 10% reduction in overall retinal thickness between mutant and control mice. **C:** Color-enhanced images of capillary beds in the adult control (top) and *Lrp5*^{tvrm111B} (bottom) retina. Note that the deep capillary bed, coded in blue in the control retina, is not present in the *Lrp5*^{tvrm111B} retina. **D:** At P8, hyaloid vessel regression is advanced in the control (left) but not in the *Lrp5*^{tvrm111B} retina (right). All images are representative of at least three mice.

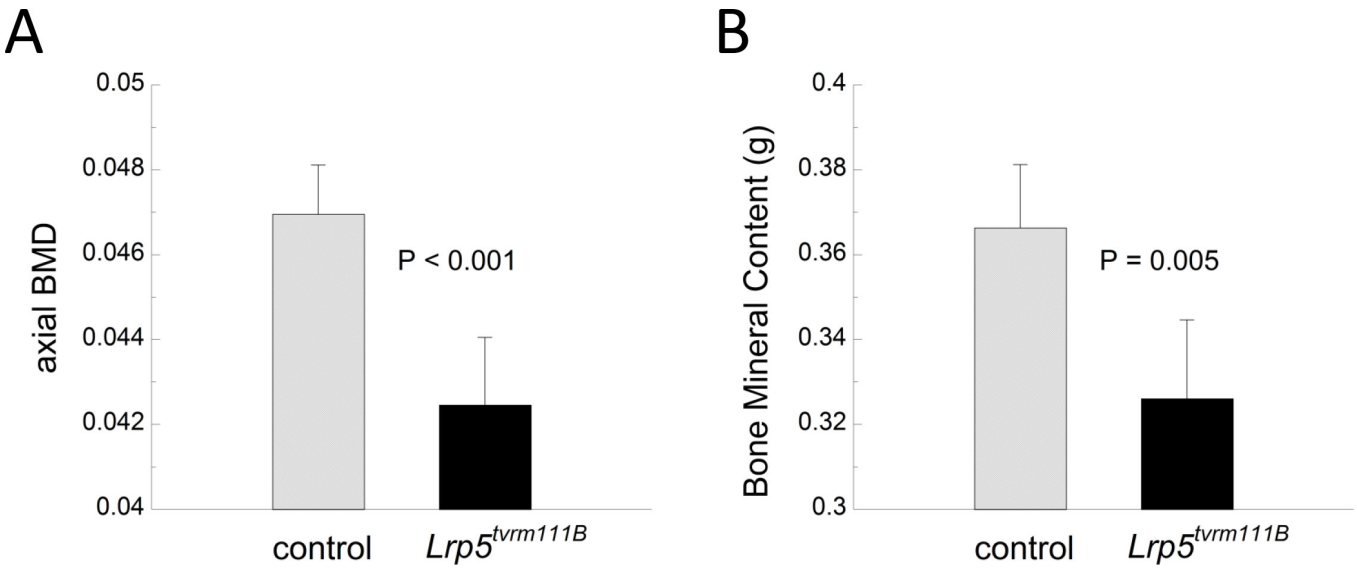

Figure 3. *Lrp5*^{tvrm111B} mutant mice exhibit reduced bone mass. **A:** Whole-body areal bone mineral density (aBMD) is reduced in *Lrp5*^{tvrm111B} mutant mice as compared to controls. **B:** This likely resulted from a decrease in bone mineral content (BMC), not a reduction in bone area (not shown). These results remained significant after correction for total tissue mass (not shown). Bars indicate average ± standard error of the mean (SEM) of five mice per group.

coding to visualize the vascular layers using Leica Application Suite software.

Dissection and staining of the hyaloid vessels: P8 pups were perfused with 4% PFA and kept at room temperature for 10 min before enucleation. After fixation and dissection, isolated hyaloid vessels were transferred to a slide and allowed to dry overnight. Hyaloid vessels were washed with PBS and stained with Hoechst 33342 (1:10,000) for 10 min (ThermoFisher), mounted in Fluoro-Gel (Electron Microscopy Sciences, Hatfield, PA), and imaged using a Zeiss AxioVision microscope (Zeiss, Thornwood, NY) and a 5× objective as previously described [29].

BMD measures: Areal BMD (aBMD) and body composition were assessed using peripheral dual-energy X-ray absorptiometry (PIXImus, GE-Lunar, Madison, WI) as previously described [30] in five homozygous *Lrp5*^{tvrm111B} and five C57BL/6J female mice at 5 months of age. We examined female mice to avoid any gender difference in BMD, noting that the BMD changes associated with *LRP5/Lrp5* mutations are not reported to differ between males and females. In short, the scans assessed whole-body (exclusive of the head) bone mineral content (BMC) and bone area. Whole-body aBMD is calculated by dividing BMC by bone area. The short-term coefficient of variation for repeat measures of total body aBMD was 8.3%.

RESULTS

The ERG phenotype in homozygous tvrm111B mice is caused by a nucleotide insertion in Lrp5: As affected *tvrm111B* mice appear generally normal, we used the ERG phenotype to map the *tvrm111B* locus. Affected mice were crossed to WT DBA/2J mice, and the resulting F1 mice were intercrossed. Of the 195 F2 progeny that were screened by ERG, 49 (25.1%) had an abnormal ERG. The *tvrm111B* phenotype was mapped to chromosome 19 using D19Mit68-rs30822407-rs30990604-D19Mit109 markers. The phenotype did not recombine with markers D19Mit68 and rs30822407, but it did recombine with rs30990604, which formed the lower chromosomal boundary for the ERG phenotype. The ERG phenotype mapped between 0 and 6.099 MB on chr19. The critical region included *Cabp4* and *Lrp5*, both of which were considered strong candidate genes due to the ERG phenotype of previously published mutants (*Cabp4* [31]; *Lrp5* [15].

We used gene expression to further evaluate these two candidate genes. No expression or coding sequence differences of *Cabp4* were observed between unaffected littermates and affected *tvrm111B* mice. A mutation in *Lrp5* was identified through SureSelect DNA capture array investigating region chr19: 3,000,001–6,207,730 (NCBI build 37 coordinates) followed by MiSeq sequencing. Probes were created every 4 bp, excluding regions that were masked due to repeats. Approximately 390,000 probes were created in this region, and they were duplicated on the array. The causal

variant (*Lrp5* c.4724_4725insG) is a single-nucleotide insertion in the final two PPPSPxS motifs at the C-terminal end of the *Lrp5* gene. This insertion adds an additional cytosine to a string of nine successive cytosines in a highly conserved guanine–cytosine (GC)-rich region. The single base insertion results in the replacement of 39 C-terminal amino acids by a new 20-amino-acid polypeptide and a premature stop codon. This mutation is identical to an independently derived ENU mutation previously described [5]. Going forward, the new mutant line will be referred to as *Lrp5*^{tvrm111B}.

Lrp5^{tvrm111B} *mice have an abnormal ERG b-wave:* Figure 1 compares strobe flash ERGs obtained from control and *Lrp5*^{tvrm111B} homozygous littermates under stimulus conditions that allow rod- and cone-mediated function to be measured. Under dark-adapted conditions (Figure 1A), both a- and b-wave amplitudes are reduced, with a much greater impact on the b-wave. Under light-adapted conditions (Figure 1B), the overall amplitude of the cone ERG is reduced.

Abnormal retinal blood vessels in Lrp5^{tvrm111B} *mice:* Together with norrin and frizzled 4, LRP5 is required for development of the deep layers of the retinal vasculature and for regression of the embryonic hyaloid vessels [5,9,15,16,23,32-35]. We conducted a series of analyses to examine these features in *Lrp5*^{tvrm111B} mice. We first used fluorescein angiography to determine whether *Lrp5*^{tvrm111B} retinal vessels were patent. While fluorescein did not leak from control vessels (Figure 2A, top), leakage, as indicated by the increasing background signal within the avascular space, was clearly noted in *Lrp5*^{tvrm111B} mice (Figure 2A, bottom). In addition, a deep vascular plexus was not visible in *Lrp5*^{tvrm111B} mice, although this plexus could be easily discerned in the controls (not shown). When we used SDOCT to examine the cross-sectional morphology, we noted that the retinal vasculature in the *Lrp5*^{tvrm111B} mice appeared to terminate (Figure 2B, white arrows) in the inner nuclear layer (Figure 2B, black arrows), which also suggested the lack of a deep vascular plexus. To examine this further, we stained whole mount retinas with 488-Fluor-conjugated isolectin to label the retinal vasculature. As shown in Figure 2C, the deep retinal layer was poorly developed in *Lrp5*^{tvrm111B} retinas in comparison to controls. When examined at P8, the hyaloid vessels persisted in *Lrp5*^{tvrm111B} retinas beyond what was observed in the control retina (Figure 2D); they also persisted in adult mutants (data not shown).

BMD: Lrp5^{tvrm111B} mice exhibit a significant decrease in whole body aBMD (Figure 3A). This results from a decrease in bone mineral content (Figure 3B), and not from a change in skeletal size (not shown). A trend toward a decrease in lumbar spinal BMD in *Lrp5*^{tvrm111B} mutant mice relative to controls

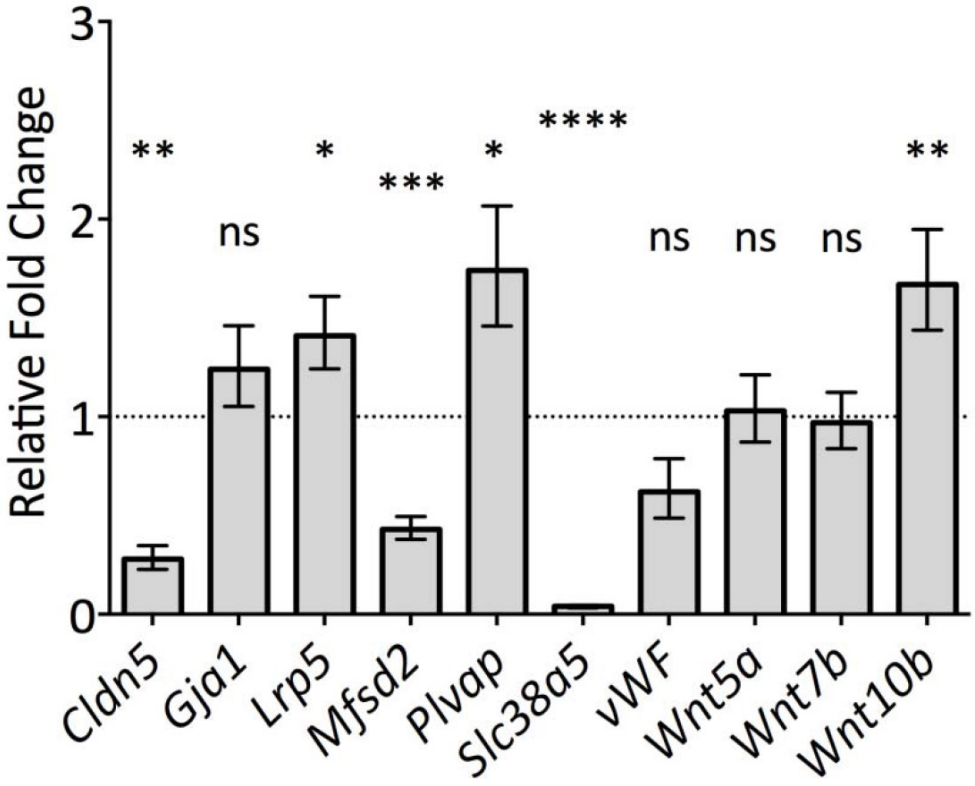

Figure 4. *Lrp5*^{tvrm111B} mutant mice exhibit differential gene expression at P8. ns: not significant; *: $p<0.05$; **: $p<0.01$; ***: $p<0.001$; ****: $p<0.0001$.

was noted; however, this was not statistically significant (control=0.0657 versus *Lrp5*^{tvrm111B}=0.0594 g/cm^2, p=0.18).

Analysis of Wnt-pathway-mediated genes: To understand the impact of the *Lrp5* mutation on Wnt signaling, we used qRT-PCR to examine expression of a series of Wnt-related genes [21]. These studies were conducted at P8, when retinal vascular development was active. Interestingly, *Lrp5* expression was significantly elevated in *Lrp5*^{tvrm111B} mutants relative to the WT (Figure 4), suggesting that a decrease in activity resulted in upregulation of *Lrp5* mRNA levels. As shown in Figure 4, we also noted that several other genes were significantly upregulated (*Plvap*, *Wnt10b*) or downregulated (*Cldn5*, *Mfsd2*, *Slc38a5*) in the *Lrp5*^{tvrm111B} retina.

DISCUSSION

In this report, we describe an autosomal recessive mouse for *Lrp5*. The *Lrp5*^{tvrm111B} was generated in a mutagenesis program that utilizes eye-specific outcome measures to identify potential mutants involving the retina [6]. The *Lrp5*^{tvrm111B} mutant was originally identified based on an abnormal ERG b-wave, a feature that was used to map the genetic location. The mutation involves the insertion of an additional cytosine in a GC-rich region. While we were not able to determine whether this additional nucleotide occurs at the start, middle, or end of a repeat of nine cytosines, the net result is a mutation that is identical to that obtained from an independent ENU mutagenesis screen by Xia and coworkers [5], suggesting that this region is highly mutable. The observed increase in transcript expression of the mutant allele of *Lrp5* is probably due to regulatory feedback mechanisms that exist under normal conditions and have been observed for other mutations, such as the homozygous *rd5* mutation in tubby (*tub*^{rd5}) allele [36].

Our studies indicate that the *Lrp5*^{tvrm111B} model shares multiple phenotypic features with previously developed *Lrp5* mutants [5,15,16]. These include defects in vascular development, such as the persistence of the hyaloid vasculature into adulthood, and incomplete growth of the deep inner retinal capillary bed. These changes are shared by mutants for *Fzd4* and *Norrin*, which control the vascular developmental processes along with LRP5 [33,35]. The incomplete development of the inner retinal blood supply is thought to underlie the abnormal ERG b-wave observed in *Lrp5* mutants, and mutants for *Fzd4* and *Norrin* [37].

Another feature of the *Lrp5*^{tvrm111B} phenotype is low BMD. Given the role of *Lrp5* in osteoblastogenesis, the reduction in bone mass in *Lrp5*$^{-/-}$ mice, associated with a decrease in bone formation and a decrease in osteoblast number, is not surprising [16]. This phenotype is reminiscent of the phenotype of OPPG patients homozygous for inactivating mutations of *LRP5* [10]. The phenotype of the *Lrp5*^{tvrm111B} mutant is less profound than that of the complete loss of function allele for *Lrp5*, but given the low–bone mass phenotypes observed in our mice, it is consistent with the hypothesis that this mutation results in a decrease in *Lrp5*/β-catenin-Wnt signaling in the osteoblast.

The *Lrp5*^{tvrm111B} was developed in a program devoted to the generation of new research mouse models. While the focus of the program is the identification of mutants affecting the eye, once established, these models are available to the research community. The *Lrp5*^{tvrm111B} mutant will be available for researchers interested in studying the role of LRP5 in the retinal vasculature, bone development, or other systems.

ACKNOWLEDGMENTS

We are grateful to Doug Howell for running the initial ERG screens associated with this project and to Gwen Sturgill-Short for technical assistance. Grant Support: This research was supported by grants from the USA National Institutes of Health (R01EY016501 and R01EY11996 to PMN; P30CA34196 The Jackson Laboratory Cancer Center Core Grant; R01EY016490, R01EY020861 and R01EY026181 to BA-A and R01EY027077 to SR), Knights Templar Eye Foundation (KTEF1401SR) and Research to Prevent Blindness (RBP1503SR), the USA Veterans Administration Medical Research Service, a Foundation Fighting Blindness Center Grant to the Cole Eye Institute, Cleveland Clinic, an unrestricted award from Research to Prevent Blindness to the Department of Ophthalmology, Cleveland Clinic Lerner College of Medicine, The Wolf Family Foundation, and the Llura and Gordon Gund Foundation.

REFERENCES

1. Takahashi JS, Pinto LH, Vitaterna MH. Forward and reverse genetic approaches to behavior in the mouse. Science 1994; 264:1724-33. [PMID: 8209253].

2. Pinto LH, Vitaterna MH, Siepka SM, Shimomura K, Lumayag S, Baker M, Fenner D, Mullins RF, Sheffield VC, Stone EM, Heffron E, Takahashi JS. Results from screening over 9000 mutation-bearing mice for defects in the electroretinogram and appearance of the fundus. Vision Res 2004; 44:3335-45. [PMID: 15536001].

3. Wang T, Zhan X, Bu CH, Lyon S, Pratt D, Hildebrand S, Choi JH, Zhang Z, Zeng M, Wang KW, Turer E, Chen Z, Zhang D, Yue T, Wang Y, Shi H, Wang J, Sun L, SoRelle J, McAlpine W, Hutchins N, Zhan X, Fina M, Gobert R, Quan J, Kreutzer M, Arnett S, Hawkins K, Leach A, Tate C, Daniel C, Reyna C, Prince L, Davis S, Purrington J, Bearden R, Weatherly J, White D, Russell J, Sun Q, Tang M, Li X, Scott L, Moresco EM, McInerney GM, Karlsson Hedestam GB,

Xie Y, Beutler B. Real-time resolution of point mutations that cause phenovariance in mice. Proc Natl Acad Sci USA 2015; 112:E440-9. [PMID: 25605905].

4. Jablonski MM, Dalke C, Wang X, Lu L, Manly KF, Pretsch W, Favor J, Pardue MT, Rinchik EM, Williams RW, Goldowitz D, Graw J. An ENU-induced mutation in Rs1h causes disruption of retinal structure and function. Mol Vis 2005; 11:569-81. [PMID: 16088326].

5. Xia C-H, Liu H, Cheung D, Wang M, Cheng C, Du X, Chang B, Beutler B, Gong X. A model for familial exudative vitreoretinopathy caused by LRP5 mutations. Hum Mol Genet 2008; 17:1605-12. [PMID: 18263894].

6. Won J, Shi LY, Hicks W, Wang J, Hurd R, Naggert JK, Chang B, Nishina PM. Mouse model resources for vision research. J Ophthalmol 2011; 2011:391384-[PMID: 21052544].

7. Won J, Shi LY, Hicks W, Wang J, Naggert JK, Nishina PM. Translational vision research models program. Adv Exp Med Biol 2012; 723:391-7. [PMID: 22183357].

8. Charette JR, Samuels IS, Yu M, Stone L, Hicks W, Shi LY, Krebs MP, Naggert JK, Nishina PM, Peachey NS. A chemical mutagenesis screen identifies mouse models with ERG defects. Adv Exp Med Biol 2016; 854:177-83. [PMID: 26427409].

9. Gong Y, Slee RB, Fukai N, Rawaki G, Roman-Roman S, Reginato AM, Wang H, Cundy T, Glorieux FH, Lev D, Zacharin M, Oexle K, Marcelino J, Suwairi W, Heeger S, Sabatakos G, Apte S, Adkins WN, Allgrove J, Arslan-Kirchner M, Batch JA, Beighton P, Black GC, Boles RG, Boon LM, Borrone C, Brunner HG, Carle GF, Dallapiccola B, De Paepe A, Floege B, Halfhide ML, Hall B, Hennekam RC, Hirose T, Jans A, Jüppner H, Kim CA, Keppler-Noreuil K, Kohlschuetter A, LaCombe D, Lambert M, Lemyre E, Letteboer T, Peltonen L, Ramesar RS, Romanengo M, Somer H, Steichen-Gersdorf E, Steinmann B, Sullivan B, Superti-Furga A, Swoboda W, van den Boogaard MJ, Van Hul W, Vikkula M, Votruba M, Zabel B, Garcia T, Baron R, Olsen BR, Warman ML. Osteoporosis-Pseudoglioma Syndrome Collaborative Group. LDL receptor-related protein 5 (LRP5) affects bone accrual and eye development. Cell 2001; 107:513-23. [PMID: 11719191].

10. Levasseur R, Lacombe D, de Vernejoul MC. LRP5 mutations in osteoperosos-pseudoglioma syndrome and high-bone-mass disorders. Joint Bone Spine 2005; 72:207-14. [PMID: 15850991].

11. Toomes C, Bottomley HM, Jackson RM, Towns KV, Scott S, Mackey DA, Craig JE, Jiang L, Yang Z, Trembath R, Woodruff G, Gregory-Evans CY, Gregory-Evans K, Parker MJ, Black GC, Downey LM, Zhang K, Inglehearn CF. Mutations in LRP5 or FZD4 underlie the common familial exudative vitreoretinopathy locus on chromosome 11q. Am J Hum Genet 2004; 74:721-30. [PMID: 15024691].

12. Jiao X, Ventruto V, Trese MT, Shastry BS, Hejtmancik JF. Autosomal recessive familial exudative vitreoretinopathy is associated with mutations in LRP5. Am J Hum Genet 2004; 75:878-84. [PMID: 15346351].

13. Boyden LM, Mao J, Belsky J, Mitzner L, Farhi A, Mitnick MA, Wu D, Insogna K, Lifton RP. High bone density due to a mutation in LDL-receptor-related protein 5. N Engl J Med 2002; 346:1513-21. [PMID: 12015390].

14. Little RD, Carulli JP, Del Mastro RG, Dupuis J, Osborne M, Folz C, Manning SP, Swain PM, Zhao SC, Eustace B, Lappe MM, Spitzer L, Zweier S, Braunschweiger K, Benchekroun Y, Hu X, Adair R, Chee L, FitzGerald MG, Tulig C, Caruso A, Tzellas N, Bawa A, Franklin B, McGuire S, Nogues X, Gong G, Allen KM, Anisowicz A, Morales AJ, Lomedico PT, Recker SM, Van Eerdewegh P, Recker RR, Johnson ML. A mutation in the LDL receptor-related protein 5 gene results in the autosomal dominant high-bone-mass trait. Am J Hum Genet 2002; 70:11-9. [PMID: 11741193].

15. Xia C-H, Yablonka-Reuveni Z, Gong X. LRP5 is required for vascular development in deeper layers of the retina. PLoS One 2010; 5:e11676-[PMID: 20652025].

16. Kato M, Patel MS, Levasseur R, Lobov I, Chang BH, Glass DA 2nd, Hartmann C, Li L, Hwang TH, Brayton CF, Lang RA, Karsenty G, Chan L. Cbfa1-independent decrease in osteoblast proliferation, osteopenia, and persistent embryonic eye vascularization in mice deficient in Lrp5, a Wnt coreceptor. J Cell Biol 2002; 157:303-14. [PMID: 11956231].

17. Justice MJ, Carpenter DA, Favor J, Neuhauser-Klaus A, Hrabé de Angelis M, Soewarto D, Moser A, Cordes S, Miller D, Chapman V, Weber JS, Rinchik EM, Hunsicker PR, Russell WL, Bode VC. Effects of ENU dosage on mouse strains. Mamm Genome 2000; 11:484-8. [PMID: 10886010].

18. Herron BJ, Lu W, Rao C, Liu S, Peters H, Bronson RT, Justice MJ, McDonald JD, Beier DR. Efficient generation and mapping of recessive developmental mutations using ENU mutagenesis. Nat Genet 2002; 30:185-9. [PMID: 11818962].

19. Hawes NL, Chang B, Hageman GS, Nusinowitz S, Nishina PM, Schneider BS, Smith RS, Roderick TH, Davisson MT, Heckenlively JR. Retinal degeneration 6 (*rd6*): A new mouse model for human retinitis *punctata albescens*. Invest Ophthalmol Vis Sci 2000; 41:3149-57. [PMID: 10967077].

20. Taylor BA, Navin A, Phillips SJ. PCR-amplification of simple sequence repeat variants from pooled DNA samples for rapidly mapping new mutations of the mouse. Genomics 1994; 21:626-32. [PMID: 7959741].

21. Hodges E, Rooks M, Xuan Z, Bhattacharjee A, Benjamin Gordon D, Brizuela L, Richard McCombie W, Hannon GJ. Hybrid selection of discrete genomic intervals on custom-designed microarrays for massively parallel sequencing. Nat Protoc 2009; 4:960-74. [PMID: 19478811].

22. Chen J, Stahl A, Krah NM, Seaward MR, Joyal J-S, Juan AM, Hatton CJ, Aderman CM, Dennison RJ, Willett KL, Sapieha P, Smith LEH. Retinal expression of Wnt-pathway mediated gene in low-density lipoprotein receptor-related protein 5 (lrp5) knockout mice. PLoS One 2012; 7:e30203-[PMID: 22272305].

23. Nordgård O, Kvaløy JT, Farmen RK, Heikkilä R. Error propagation in relative real-time reverse transcription polymerase chain reaction quantification models: the balance between

accuracy and precision. Anal Biochem 2006; 356:182-93. [PMID: 16899212].

24. Peachey NS, Pearring JN, Bojang P Jr, Hirschtritt ME, Sturgill-Short GM, Ray TA, Furukawa T, Koike C, Goldberg AFX, Shen Y, McCall MA, Nawy S, Nishina PM, Gregg RG. Depolarizing bipolar cell dysfunction due to a *Trpm1* point mutation. J Neurophysiol 2012; 108:2442-51. [PMID: 22896717].

25. Bell BA, Kaul C, Hollyfield JG. A protective eye shield for prevention of media opacities during small animal ocular imaging. Exp Eye Res 2014; 127:280-7. [PMID: 25245081].

26. Bell BA, Kaul C, Bonilha VL, Rayborn ME, Shadrach K, Hollyfield JG. The BALB/c mouse: Effect of standard vivarium lighting on retinal pathology during aging. Exp Eye Res 2015; 135:192-205. [PMID: 25895728].

27. Paques M, Simonutti M, Roux MJ, Picaud S, Levavasseur E, Bellman C, Sahel JA. High resolution fundus imaging by confocal scanning laser ophthalmoscopy in the mouse. Vision Res 2006; 46:1336-45. [PMID: 16289196].

28. Thévenaz P, Ruttimann UE, Unser M. A pyramid approach to subpixel registration based on intensity. IEEE Trans Image Process 1998; 7:27-41. [PMID: 18267377].

29. Rao S, Lobov IB, Vallance JE, Tsujikawa K, Shiojima I, Akunuru S, Walsh K, Benjamin LE, Lang RA. Obligatory participation of macrophages in an angiopoietin 2-mediated cell death switch. Development 2007; 134:4449-58. [PMID: 18039971].

30. Ackert-Bicknell CL, Shockley KR, Horton LG, Lecka-Czernik B, Churchill GA, Rosen CJ. Strain-specific effects of rosiglitazone on bone mass, body composition, and serum insulin-like growth factor-I. Endocrinology 2009; 150:1330-40. [PMID: 18948404].

31. Haeseleer F, Imanishi Y, Maeda T, Possin DE, Maeda A, Lee A, Rieke F, Palczewski K. Essential role of Ca^{2+}-binding protein 4, a Cav1.4 channel regulator, in photoreceptor synaptic function. Nat Neurosci 2004; 7:1079-87. [PMID: 15452577].

32. Richter M, Gottanka J, May CA, Welge-Lüssen U, Berger W, Lutjen-Drecoll E. Retinal vasculature changes in Norrie disease mice. Invest Ophthalmol Vis Sci 1998; 39:2450-7. [PMID: 9804153].

33. Xu Q, Wang Y, Dabdoub A, Smallwood PM, Williams J, Woods C, Kelley MW, Jiang L, Tasman W, Zhang K, Nathans J. Vascular development in the retina and inner ear: control by Norrin and Frizzled-4, a high-affinity ligand-receptor pair. Cell 2004; 116:883-95. [PMID: 15035989].

34. Luhmann UF, Lin J, Acar N, Lammel S, Feil S, Grimm C, Seeliger MW, Hammes HP, Berger W. Role of the Norrie disease pseudoglioma gene in sprouting angiogenesis during development of the retinal vasculature. Invest Ophthalmol Vis Sci 2005; 46:3372-82. [PMID: 16123442].

35. Ye X, Wang Y, Cahill H, Yu M, Badea TC, Smallwood PM, Peachey NS, Nathans J. Norrin, frizzled-4, and Lrp5 signaling in endothelial cells controls a genetic program for retinal vascularization. Cell 2009; 139:285-98. [PMID: 19837032].

36. Noben-Trauth K, Naggert JK, North MA, Nishina PM. A candidate gene for the mouse mutation tubby. Nature 1996; 380:534-8. [PMID: 8606774].

37. Pardue MT, Peachey NS. Mouse b-wave mutants. Doc Ophthalmol 2014; 128:77-89. [PMID: 24395437].

Articles are provided courtesy of Emory University and the Zhongshan Ophthalmic Center, Sun Yat-sen University, P.R. China. The print version of this article was created on 18 March 2017. This reflects all typographical corrections and errata to the article through that date. Details of any changes may be found in the online version of the article.